EarthArXiv Coversheet

Global Alpine Treeline Elevational Transects

Chenyang Wei[1,2], Adam M. Wilson[2]

1. Department of Evolution, Ecology and Organismal Biology, The Ohio State University, 318 W. 12th Avenue, 300 Aronoff Laboratory, Columbus, OH 43210, USA

2. Department of Geography, University at Buffalo, The State University of New York, Buffalo, NY 14261, USA

Author contact:

Chenyang Wei — Email: ChenyangWei.CWei@gmail.com (corresponding author)

Adam M. Wilson — Email: adamw@buffalo.edu

Preprint and peer-review status:

This document is a non-peer-reviewed preprint submitted to EarthArXiv. The manuscript has been submitted to Scientific Data for peer review. Upon acceptance, citation details and DOI will be updated in the preprint record.

Preprint date: October 23, 2025

Title
Global Alpine Treeline Elevational Transects

Authors
Chenyang Wei[1,2], Adam M. Wilson[2]

Affiliations
1. Department of Evolution, Ecology and Organismal Biology, The Ohio State University, 318 W. 12th Avenue, 300 Aronoff Laboratory, Columbus, OH 43210, USA

2. Department of Geography, University at Buffalo, The State University of New York, Buffalo, NY 14261, USA

Corresponding author: Chenyang Wei (ChenyangWei.CWei@gmail.com)

Abstract
The Alpine Treeline Ecotone (ATE) is an important ecological transition zone at the juncture of montane forests and alpine tundra. It serves as a crucial habitat for diverse species and a sensitive indicator of climate change. Consistent characterization of the elevational gradients of ATE is challenging due to complex topography and data limitations. This study introduces a comprehensive geospatial dataset delineating 2.3 million elevational transects within global ATEs. The dataset integrates global climatology with key environmental attributes, such as elevation, landforms, hydrology, and land cover. These transects effectively map the ecological transition from dense montane forests to barren, higher-altitude ridges. Their spatial flexibility facilitates standardized comparative analysis of ATEs, effectively bridging the gap between local field studies and global assessments in alpine research. The dataset can be employed to model the elevational distribution of ecosystem properties within ATEs, track the temporal changes of environmental factors along the ATE's elevational gradients, and forecast the specific, enduring effects of climate change on mountain ecosystems worldwide.

Background & Summary
Environmental conditions such as air temperature and atmospheric pressure undergo significant changes with elevation. In mountainous regions, these variations result in short growing seasons, limited soil moisture, and brief periods without snow cover in alpine zones[1,2], exerting both direct and indirect impacts on the elevation-based characteristics of local communities and ecosystems[3,4]. For instance, these conditions contribute to reduced wood production in alpine areas, as highlighted by Körner[5].

A notable ecological transition occurs as the mean growing season air temperature drops from about 10℃ to roughly 3.5℃ ascending from the upper montane thermal belt to the lower alpine zone[6]. This shift, spanning an elevation increase of approximately one kilometer[7,8] or a lateral movement of 0.6-2.7 km along slopes of 20° to 60°, sees a landscape transition from tree-dominated areas to those chiefly characterized by lower-stature vegetation such as shrubs, grasses, and forbs. This vegetational shift delineates an important ecological boundary between the uppermost montane forests and the treeless alpine tundra, known as the "Alpine Treeline Ecotone (ATE)"[9,10]. As one of the most striking manifestations of increasing elevation in mountain ecosystems[11], the ATE is theoretically related to the cold tolerance limit within the fundamental niche of tree species[12,13]. Investigating the elevational gradients in ecosystem properties within this essential transition zone provides crucial insights into the ecological dynamics of mountainous regions in the context of global climate change[14].

Elevational Transects in Alpine Treeline Ecotone Research

Field studies frequently utilize linear transects to explore vegetation growth and variability in alpine treeline ecotones across different elevations[15–23]. These transects, typically established on a single hillside, account for key spatial factors such as elevation, slope, and aspect in mountainous terrains. The use of elevational transects in data analysis offers several advantages for studying environmental variations within ATEs, while mitigating issues inherent to spatially gridded datasets (refer to Table 1). For further details on the limitations of grid-based data in ATE research, see Supplementary File 1 and Supplementary Fig. 1.

No.	Gridded datasets		Elevational transects
	Descriptions	**Examples in Supplementary Fig. 1**	**Descriptions**
1	Risk of overlooking sub-pixel variations and obscuring spatial patterns in ATEs due to coarse resolution.	Pixels 6 and 7.	Consistent slope-specific data acquisition.
2	Inconsistent spatial representation of ecological transitions in varied terrains.	Pixels 2-5.	Flexible length adjustment for precise data collection on varying hillsides.
3	Data analysis skewed towards lower elevations in mountainous regions.	Pixel 8.	Consistent data collection at each elevation due to uniform transect width.
4	Streamlined spatial operations (e.g., aggregation and partitioning) facilitated by consistent pixel layout.	N/A.	Challenging spatial operations due to varying transect layouts.
5	Ease of comparing and integrating analyses from various datasets on similar themes or locations.	N/A.	Additional operations (such as spatial thinning or aggregation) are necessary for comparing or integrating transects with other gridded datasets.

Table 1. Comparative Analysis of Gridded Datasets Versus Elevational Transects in Alpine Treeline Ecotone (ATE) Research.

Firstly, by spanning from lower to higher elevations on one slope, each transect provides consistent, slope-specific data, eliminating potential confusion from neighboring topographical features. Secondly, the length of these transects can be easily adjusted to fit the hillside's dimensions, offering flexible yet precise data collection. Thirdly, the uniform width of transects ensures standardized data collection at each elevation, allowing for consistent environmental variable analysis. Furthermore, transect-based findings can be effectively compared with localized field data collected along the elevational gradient, enhancing validation and comparison across a broad area.

In this study, we introduce a novel dataset consisting of 2.3 million precisely defined elevational transects, each 90 meters wide, located within alpine treeline ecotones across the globe (https://zenodo.org/records/10739392). These transects are established by integrating global climatology with topography, landforms, hydrology, and land cover to map the ecological shift from barren mountain ridges to the adjacent lower-elevation dense forests. They capture the intricate spatial patterns and topographical nuances of ATEs at a local scale. Our method provides an alternative approach to grid-based data in areas of complex topography, facilitating uniform comparative studies of alpine treeline ecotones worldwide. It also bridges the gap between localized field research and global-scale ecological and environmental estimations in mountain regions. The creation of this dataset primarily utilized Google Earth Engine, an accessible, cloud-based platform offering high-performance computing capabilities[24]. To

the best of our knowledge, this represents the first endeavor to automate the construction of such transects along the elevational gradients within ATEs on a global scale.

The geospatial dataset described in this article is particularly valuable for several applications. It is ideal for analyzing how ecosystem characteristics, such as biodiversity and primary productivity, vary with elevation in alpine treeline ecotones. Additionally, it allows for the monitoring of changes over time in environmental factors like air temperature and soil organic matter, across the elevational range of ATEs. This dataset is also useful for predicting the effects of climate change on mountain ecosystems in the long term, such as shifts in species distribution and alterations in community structure. Moreover, the methodology employed in creating this dataset can be adapted to study other geospatial variables like precipitation, soil moisture, vegetation coverage, and water depth, by establishing transects along their gradients.

Methods

The methodology for developing elevational transects in alpine treeline ecotones encompassed four primary stages: First, we identified broad extents of ATEs across various mountainous regions worldwide. Second, we delineated specific landscape units within these alpine treeline ecotones. Third, we established transect centerlines within these units. Finally, we selected the transects with the steepest elevation gradients for detailed study. The JavaScript code outlining each step in constructing elevational transects, using Olympic National Park, Washington, USA as a case study and facilitated through Google Earth Engine, can be accessed at https://zenodo.org/records/17428155. The final data product includes two key components: a) a vector dataset representing the elevational transects across global ATEs, and b) a vector dataset detailing the geometric centroid of each individual elevational transect.

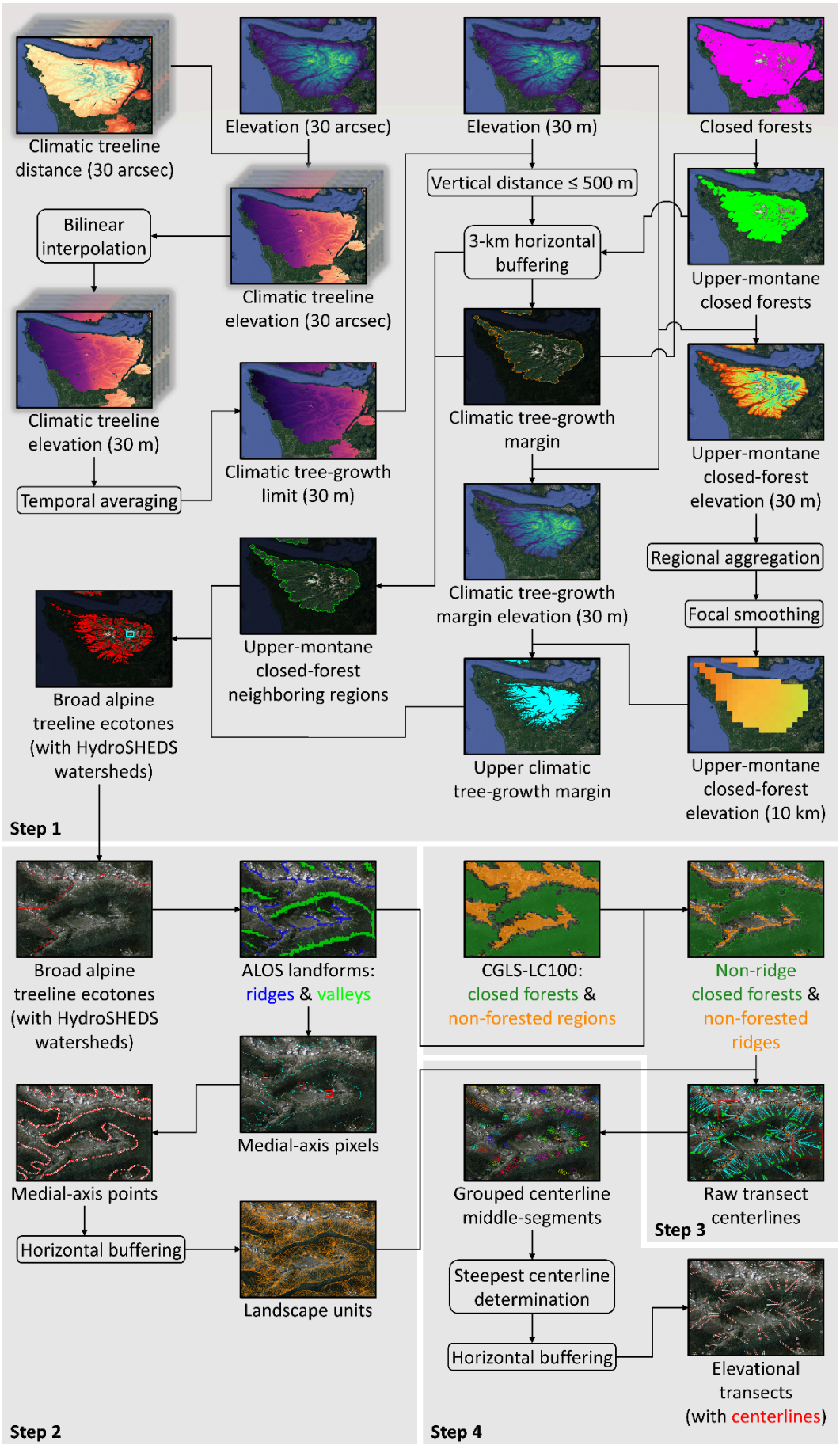
Climatic treeline distance (30 arcsec)
Elevation (30 arcsec)
Elevation (30 m)
Closed forests
Vertical distance ≤ 500 m
Bilinear interpolation
Climatic treeline elevation (30 arcsec)
3-km horizontal buffering
Upper-montane closed forests
Climatic treeline elevation (30 m)
Climatic tree-growth limit (30 m)
Climatic tree-growth margin
Upper-montane closed-forest elevation (30 m)
Temporal averaging
Regional aggregation
Climatic tree-growth margin elevation (30 m)
Focal smoothing
Upper-montane closed-forest neighboring regions
Broad alpine treeline ecotones (with HydroSHEDS watersheds)
Upper climatic tree-growth margin
Upper-montane closed-forest elevation (10 km)
Step 1
Broad alpine treeline ecotones (with HydroSHEDS watersheds)
ALOS landforms: ridges & valleys
CGLS-LC100: closed forests & non-forested regions
Non-ridge closed forests & non-forested ridges
Medial-axis pixels
Medial-axis points
Grouped centerline middle-segments
Raw transect centerlines
Step 3
Horizontal buffering
Landscape units
Steepest centerline determination
Horizontal buffering
Elevational transects (with centerlines)
Step 2
Step 4

Fig. 1 Workflow for Constructing Alpine Treeline Elevational Transects (ATETs) in Olympic National Park, Washington, USA. The process involves four steps. **Step 1:** Identify broad extents of Alpine Treeline Ecotones (ATEs) in mountainous areas. **Step 2:** Generate circular landscape units within these ATEs for subsequent data processing. **Step 3:** Establish an elevational transect centerline in each landscape unit. **Step 4:** Identify the steepest transects, each 90 meters wide, within the alpine treeline ecotones. In particular, the area highlighted for "Steps 2-4" corresponds to the cyan-colored rectangle displayed in the "Broad alpine treeline ecotones (with HydroSHEDS watersheds)" panel of "Step 1."

Step 1: Alpine Treeline Ecotone Identification

The uniformity of bioclimatic constraints acting on alpine treeline ecotones suggests that the mechanisms shaping ATE distributions are broadly similar worldwide[1,25]. The first step was to define the general scope of ATEs across global mountain regions. We began by selecting high, scattered high, low, and scattered low mountain classes from the 250-m global Hammond landform dataset[26,27] as our primary study domain. Our definition of the alpine treeline ecotone, for this study, encompasses both the theoretical and observed treelines in the world's mountains[9]. These respectively represent the coldest limit of the fundamental tree-growth niche and the upper boundary of the realized tree-growth niche[13]. To adequately capture these dual aspects of tree niches within the study area, we identified two critical features for our broad ATE scope (refer to "Step 1" in Fig. 1): 1) a climatic setting at the verge of tree viability, and 2) a geographical position proximal to, yet surpassing, the upper-montane closed forest in elevation.

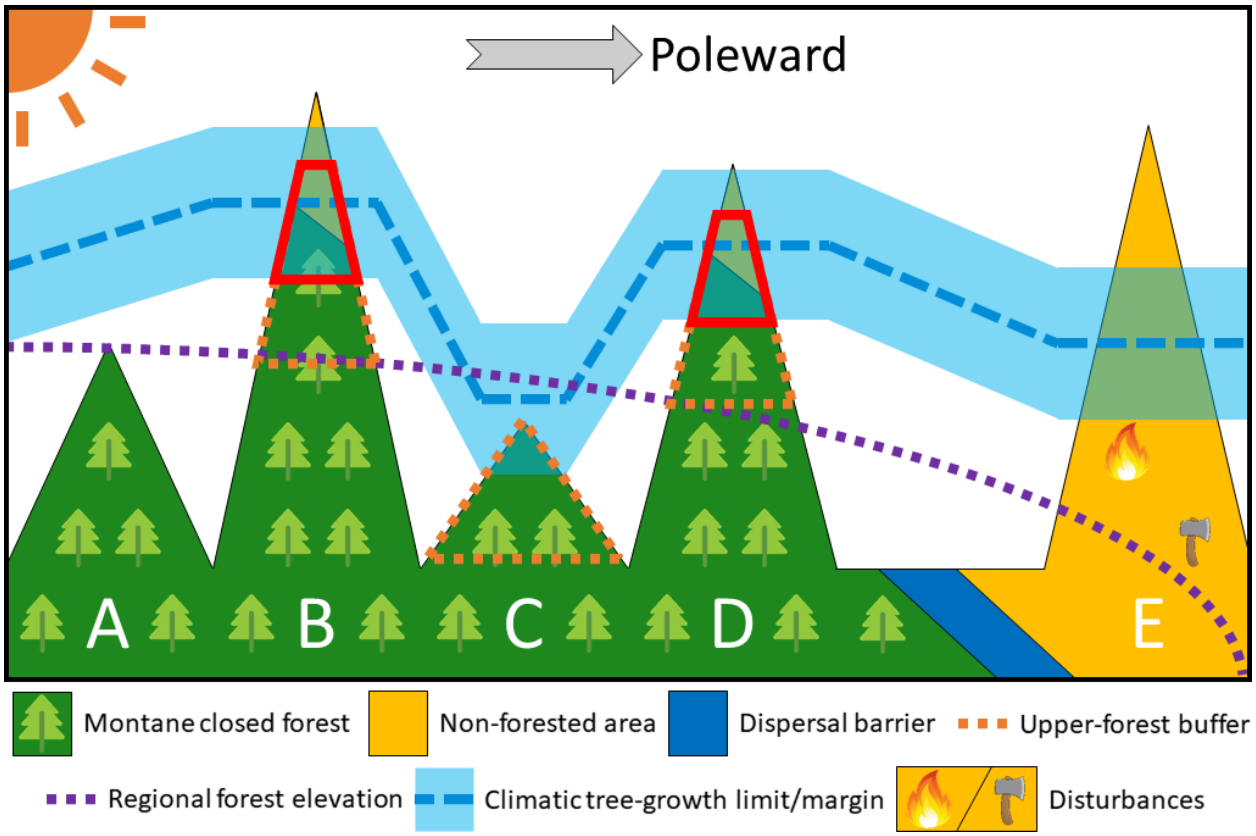

Fig. 2 Illustration of Broad Alpine Treeline Ecotones (ATEs) in a Simplified Mountainous Landscape. This figure depicts three primary land cover types: montane closed forests, non-forested areas, and dispersal barriers. The dashed blue line and corresponding blue-shaded areas represent the theoretical limit and margin of tree growth in these environments based on climate data from 1979 to 2013. The dotted purple line delineates the elevational boundary of upper-montane closed forests on a

regional scale. Orange-dotted polygons, partially overlapping with red in Mountains B and D, indicate areas adjacent to these forests. Icons of fire and an ax in Mountain E highlight regions potentially impacted by human or natural disturbances like wildfire and logging, independent of latitude. Red polygons across the landscape mark the determined broad ATEs, demonstrating their distribution and extent in various mountain settings.

Step 1.1: Identifying the Edge of Trees' Fundamental Niche
We delineated the lower temperature limit for tree growth using the climate-based model of treeline elevation by Paulsen and Körner[2]. This approach was established from 376 global tree life-form boundaries to identify the requisite conditions for tree growth: a minimum 94-day growing season with daily mean air temperatures above 0.9°C and a seasonal average air temperature of 6.4°C. Building on this, the Climatologies at High resolution for the Earth's Land Surface Areas (CHELSA) treeline distance dataset by Karger et al.[28,29] was integrated. This dataset provides annual elevational distances from the land surface to the theoretical tree-growth limit at a resolution of 30-arcsec (approx. 1 km at the equator) globally from 1979 to 2013. Specifically, if a 30-arcsec pixel lies below the local theoretical treeline elevation in a given year, its CHELSA treeline distance is marked as positive; otherwise, it's negative (see red/orange and blue areas in Fig. 1's "Climatic treeline distance (30 arcsec)" panel, respectively).

To identify the theoretical treeline elevation from 1979 to 2013 within our study area, we combined the annual CHELSA treeline distance with terrain elevation from the Global Multi-resolution Terrain Elevation Data 2010 (GMTED2010)[30]. The derived theoretical treeline elevation, illustrated in Fig. 1's "Climatic treeline elevation (30 arcsec)" panel, exhibited minimal noise and distinct boundaries. We then performed bilinear interpolation resampling to enhance the resolution to 30 m (displayed in Fig. 1's "Climatic treeline elevation (30 m)" panel). Notably, this approximation doesn't account for local topographical factors and serves primarily to define the study's initial scope. Additionally, considering the significant temporal climatic fluctuations in mountain regions[31,32], we calculated the temporal average of these treeline elevations at each 30-m pixel to determine the long-term theoretical tree-growth limit (referenced in Fig. 1's "Climatic tree-growth limit (30 m)" panel and indicated by the dashed blue line in Fig. 2).

Next, using the ALOS World 3D-30m (AW3D30) global Digital Surface Model (DSM) V3.2[33–35], known for its relatively small uncertainty and high accuracy[36], we identified regions near the theoretical treeline. Given the approximate one-kilometer altitudinal extent of the upper montane and lower alpine bioclimatic zones[6–8], we focused on 30-m pixels within a 500 m vertical and 3 km horizontal range from the theoretical tree-growth limit, marking these as the long-term theoretical tree-growth margin (visible in Fig. 1's "Climatic tree-growth margin" panel and as blue-shaded zones in Mountains B-E in Fig. 2). This step excluded areas far from the theoretical treeline, like Mountain A in Fig. 2, effectively isolating the fundamental niche edge of tree species for subsequent analysis.

Step 1.2: Identifying the Edge of Trees' Realized Niche
The upper range limit of trees' realized niche typically lies above the neighboring observed upper-montane closed forests, shaped by bioclimatic factors. These forests' elevational variance is substantial due to complex topography and environmental influences at local (like individual slopes) and regional (such as mountain ranges) scales. For example, in the northern hemisphere, montane closed forests often reach higher elevations on south-facing slopes compared to their north-facing counterparts, as evident in Mountains B and D in Fig. 2 (upper dark-green areas). In contrast, in specific regions like the Hengduan Mountains, China, treelines on sun-facing slopes can be lower due to local environmental factors, such as the monsoon climate[37,38]. Our approach integrates local and regional data to accurately represent the upper boundary of trees' realized niche.

To identify the upper-montane closed forest locally, we used the "discrete classification" from the Copernicus Global Land Service's Dynamic Land Cover (CGLS-LC100) V3.0.1 data[39], which provides detailed global land cover information from 2015 to 2019 based on the UN Land Cover Classification System[40]. Thanks to its hierarchical structure, this system derives unique and unambiguous standardized land cover classes and allows for detailed categorization of forest types[39]. We specifically focused on six forest types with over 70% canopy cover, ensuring that areas consistently classified as closed forests during 2015-2019 were included to minimize misclassification errors (Fig. 1, "Upper-montane closed forests" panel; Fig. 2, blue-shaded dark-green zones in Mountains B-D).

Regionally, we considered that air temperature typically drops by about 0.1℃ per 12.3 km poleward in mid-latitudes[41]. To capture this variability in tree niche edges across mountain landscapes, we used a 10-km spatial unit for analysis. The process involved local extraction of upper-montane closed-forest elevations at 30-m resolution (illustrated in Fig. 1's "Upper-montane closed-forest elevation (30 m)" panel), regional averaging of these 30-m elevations within each 10-km pixel, and focal smoothing to mitigate local variations (Fig. 1, "Upper-montane closed-forest elevation (10 km)" panel; Fig. 2, the dotted purple line). In particular, to align with the median size of major mountain systems worldwide (approx. 49,638.8 km^2), as per the Global Mountain Biodiversity Assessment (GMBA) Mountain Inventory V2.0 database[42,43], we calculated the focal mean of the aggregated 10-km elevations within each ten-pixel circular kernel (approx. 31,415.9 km^2). Subsequently, as depicted in Fig. 1's "Upper climatic tree-growth margin" panel, we excluded the theoretical tree-growth margin below the focal average elevation, such as the blue-shaded zone in Mountain C in Fig. 2.

Additionally, we acknowledged that trees might be absent from potential treeline areas due to local factors like natural disturbances, dispersal barriers, soil status, and human interventions[12,13]. To address this distributional difference between the fundamental and realized niche edges of trees, considering the potential horizontal range of the upper montane and lower alpine thermal belts (approx. 0.6-2.7 km along slopes of 20° to 60°), we identified the upper theoretical tree-growth margin within 3 km of upper-montane closed forests (Fig. 1, "Upper-montane closed-forest neighboring regions" panel; Fig. 2, dotted orange polygons (partially overlapped with red polygons in Mountains B and D)). Finally, using the Hansen Global Forest Change V1.7 data[44], we excluded in-land water from our study, defining broad extents of alpine treeline ecotones worldwide at a 30-m resolution. These identified areas represent the ecological shift from upper-montane closed forest to the higher-elevation treeless alpine tundra (Fig. 1, the "Broad alpine treeline ecotones (with HydroSHEDS watersheds)" panel of "Step 1"; Fig. 2, red polygons). All following analyses are limited to this domain.

Step 2: Landscape Unit Determination

To effectively process the high-resolution data necessary for global-scale transect creation, we utilized the advanced geospatial processing power of Google Earth Engine[24]. We divided the identified alpine treeline ecotones into finely detailed watersheds, classified as "Level 12," using the Hydrological Data and Maps Based on Shuttle Elevation Derivatives at Multiple Scales (HydroSHEDS) dataset[45,46]. The red outlines of these watersheds are visible in the "Broad alpine treeline ecotones (with HydroSHEDS watersheds)" panel of "Step 2" in Fig. 1. This division enabled us to carry out parallel computations in Google Earth Engine, bypassing the need to arbitrarily split the broad ATEs. It also ensured that data for each transect was exclusively sourced from a single watershed, thus avoiding cross-contamination of data from neighboring areas.

Given the complex topography of alpine treeline ecotones, including varying slopes and aspects, it's crucial to establish transects at the hillside level. This ensures they capture local ecological and environmental differences along the elevation gradient without blending data from multiple hillsides. As depicted in Fig. 1 ("Step 2") and Fig. 3a,b, we identified landscape units at the hillside scale within the broad ATEs for subsequent transect generation processes.

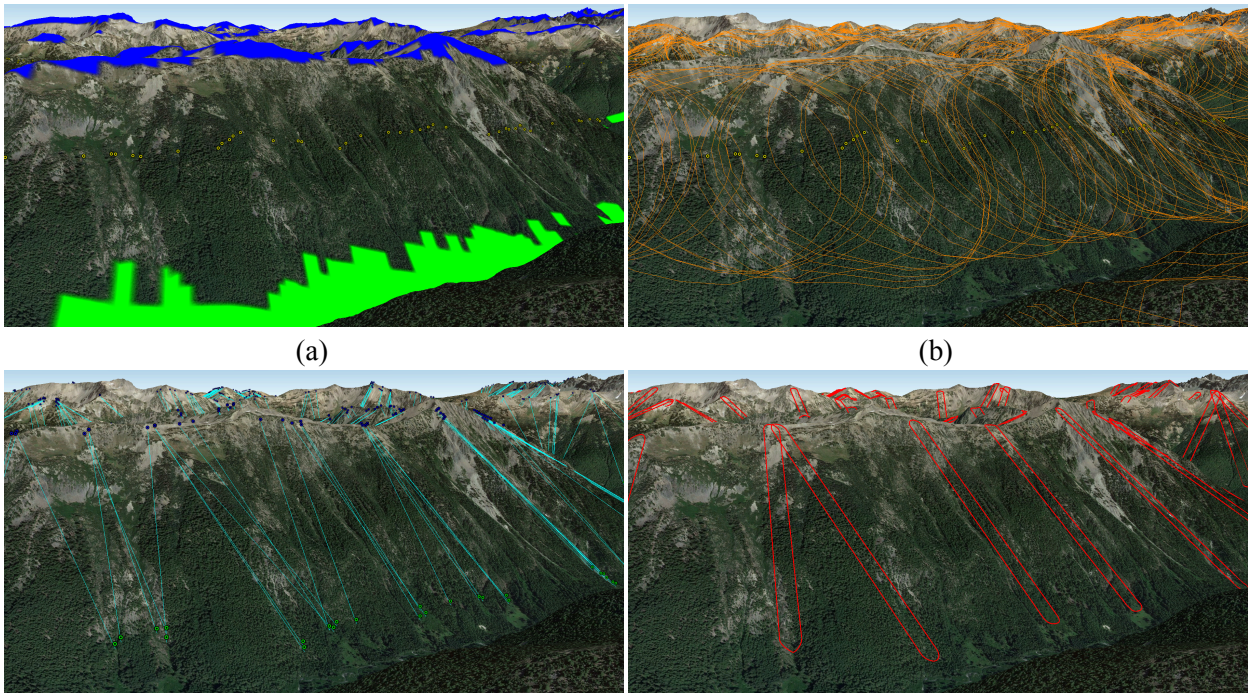

Fig. 3 Three-Dimensional Depiction of Elevational Transect Development Within the Broad Alpine Treeline Ecotone (ATE) on a Designated Hillside in Olympic National Park, Washington, USA. This hillside is indicated by the white rectangle in Supplementary Fig. 1f. Panel **(a)** depicts the ridge (in blue) and valley (in green) landforms, alongside the geometric centroids (yellow points) of the grouped 30-m pixels on their medial axis. Panel **(b)** illustrates the identified landscape units (orange circles) and their medial-axis geometric centroids (yellow points). Panel **(c)** shows the lowest non-ridge closed forest locations (green points), the highest non-forested ridge areas (blue points), and the central line (cyan lines) of the elevational transects within each landscape unit. Panel **(d)** presents the finalized Alpine Treeline Elevational Transects (ATETs), each with a width of 90 m (represented as red polygons).

For defining landscape units within each HydroSHEDS watershed, we first identified key landform categories - ridges and valleys - within the study area. This was done using the 90-m Global ALOS Landform dataset[47], as shown in Fig. 1 (the "ALOS landforms: ridges & valleys" panel) and Fig. 3a (blue for ridges, green for valleys). The ridge landform included various types of peaks, ridges, and mountain divides, excluding the "cliff" category due to its irregular spatial distribution. The valley category encompassed normal and narrow valleys. We also excluded high-latitude areas (> 60° N/S) lacking valid data from the ALOS Landform dataset.

Next, we identified 30-m pixels along the central axis between ridges and valleys within the broad ATEs (as shown by the cyan areas in Fig. 1's "Medial-axis pixels" panel). The distance from each identified pixel to its nearest ridge or valley was termed "unit distance." To enhance the representativeness of landscape units, we grouped medial-axis pixels based on edge-sharing or diagonal connection and uniform unit distance (indicated by red rectangles in Fig. 1's "Medial-axis pixels" panel).

Finally, we established local landscape units at the geometric center of each pixel group (illustrated by yellow points in Fig. 3a,b). We marked a circle with a radius equal to the unit distance at these centroids. As shown by the orange circles in Fig. 3b, the boundaries of these landscape units effectively encompass the transition zones from highlands to lowlands, while avoiding overlap across multiple hills or slopes.

The circular shape of these units enables precise representation of elevational gradients from any direction at the hillside scale.

Step 3: Transect Centerline Construction
In this phase, we developed the centerline of an elevational transect within each landscape unit globally (refer to "Step 3" in Fig. 1). Initially, we gathered land cover data from the CGLS-LC100 product, identifying closed forests (tree canopy > 70%) within the broad ATEs as the potential start of transects, following the methodology from Step 1. Additionally, we pinpointed alpine tundra, marked by non-forested land, by locating areas without closed or open forests (tree canopy = 15-70%) during 2015-2019, as per the CGLS-LC100 dataset.

Next, we recognized the importance of ridges in mountain landscapes. Ridges, serving as natural dividers in hillslopes, exhibit distinct environmental attributes (like solar exposure and wind conditions). For mountain flora, these ridges often represent the upper limit of their habitat. Utilizing the ALOS Landform dataset, we distinguished ridges from other landforms in alpine treeline ecotones.

Then, focusing on identifying the transition in vegetation productivity, we combined land cover data to locate areas with closed forests (not on ridges) and non-forested ridges within the broad ATEs. For each landscape unit encompassing these regions, we identified the lowest point in non-ridge closed forests (illustrated as green points in Fig. 3c) and the highest non-forested ridge (blue points in Fig. 3c), using the AW3D30 global DSM V3.2 dataset. To ensure accuracy, we excluded non-forested ridges potentially resulting from disturbances like wildfires, logging, or mining by only considering transect endpoints where the upper point (the highest non-forested ridge) was above the lower point (the lowest non-ridge closed forest).

Finally, within each landscape unit, we established a transect centerline as a straight line linking these two endpoints. As shown by the cyan lines in Fig. 3c, these centerlines typically stretch from ecologically productive lowlands to less productive high-altitude areas within alpine treeline ecotones.

Step 4: Steepest Transect Selection
Upon completion of Step 3, it became apparent that many transect centerlines were closely situated. To address this, Step 4 focused on identifying the steepest centerlines. This step aimed to minimize redundancy and ensure the transects accurately represented the local terrain.

Unlike endpoints that were influenced by specific topographical features (such as peaks and valleys, indicated in the lower-right and upper-left red rectangles of the "Raw transect centerlines" panel in Fig. 1), the clustering of medial-axis pixels largely influenced the middle segments of transect centerlines. This clustering could result in redundant transects. To manage this, we first pinpointed a middle segment near each centerline's geometric centroid. Given the varying lengths of centerlines, we defined the middle segment as a quarter of its total length (illustrated in the "Grouped centerline middle-segments" panel of "Step 4" in Fig. 1).

Next, we created a 90-m horizontal buffer around each middle segment (as depicted in the same panel of Fig. 1), this being the predetermined width for our transects. For overlapping middle-segment buffers, we chose the centerline with the largest elevation difference between its endpoints (highlighted by red lines in the "Elevational transects (with centerlines)" panel of "Step 4" in Fig. 1). A 45-m horizontal buffer was then applied around each chosen centerline, forming a 90-m wide elevational transect (equivalent to three 30-m pixels, shown as white polygons in the same panel of Fig. 1). This grouping method ensured that the distance between middle segments of adjacent transects exceeded 90 m, as demonstrated by red polygons in Fig. 3d and Supplementary Fig. 1f.

Additionally, given the potential horizontal extent of the upper montane and lower alpine regions (approx. 0.6-2.7 km along slopes of 20° to 60°), we selected transects ranging from 300 m to 3 km in length to prevent excessively long transects, which may result from gaps in high-latitude regions within the ALOS Landform dataset. This range also ensured each transect spanned at least thirty 30-m pixels. For mountain range classification, we utilized the GMBA Mountain Inventory V2.0 database, which provides detailed information on major mountain systems worldwide. We extracted basic data (ID, name, region, and centroid coordinates) for each GMBA mountain range intersecting our transects' centroids and appended this to the transect data, as detailed in Table 2. Transects with centroids outside the defined "Broad" GMBA mountainous areas were excluded from our final dataset.

Data Records

Alpine Treeline Elevational Transects_v1.0 (ATET_v1.0)

The ATET_v1.0 dataset (refer to Table 2), comprises 2,312,022 polygons. These polygons delineate the spatial bounds of elevational transects within globally identified alpine treeline ecotones in mountainous regions. The dataset's attributes are divided into three categories:

1) **Geometric, Geographical, and Ecological Properties:** This includes the horizontal length, elevation range, average slope angle, the locations of the transects' geometric centroids and centerline endpoints, and ecological metrics like average vegetation canopy height and greenness index for each transect segment (as illustrated by the red and blue polygons in Fig. 6d).
2) **Watershed Information:** Each transect is linked to the finest level ("Level 12") of the HydroSHEDS watershed, denoted by "HYBAS_ID" in Table 2. This linkage, based on the transect's geometric centroid, facilitates efficient parallel computing on Google Earth Engine and aids in aggregating elevational transects within these watersheds (visible in Fig. 4b and Fig. 5b).
3) **Mountain Range Information:** Variables starting with "GMBA_" provide basic information about the "Broad" GMBA mountain ranges where each transect's centroid is located. As depicted in Fig. 4c and Fig. 5c, these attributes enable the compilation of data from individual transects to the level of mountain ranges.

Attributes			Objects/File Size
Type	**Name**	**Description**	
Elevational Transect	ET_ID	**Elevational Transect Identifier:** Unique identifier for each transect, linking it to its geometric centroid.	**ATET_v1.0 (Alpine Treeline Elevational Transects_v1.0)** **Type:** ESRI Shapefile **Content:** Consists of 2,312,022 polygons. Each polygon represents the spatial boundaries of an elevational transect. **File Size:** 2.71 GB **ATEC_v1.0 (Alpine Treeline Elevational Transect Centroids_v1.0)** **Type:** ESRI Shapefile **Content:** Includes 2,312,022 points, each indicating the geometric centroid of an elevational transect. **File Size:** 1.72 GB **ATET_ATEC_v1.0** **Type:** OGC GeoPackage **Content:** Comprises the two vector datasets of "Alpine Treeline Elevational Transects_v1.0" and
	Elv_Range	**Elevation Difference:** The vertical distance in meters between the upper and lower endpoints of the transect's centerline. Represented as a positive integer.	
	H_Length	**Horizontal Length:** The length of the transect's centerline in meters, ranging from 300 m to 3 km.	
	Avg_Slope	**Average Slope:** The slope of the transect's centerline in degrees, calculated using "Elv_Range" and "H_Length" attributes.	
	Ctr_Lon	**Geometric Centroid Longitude:** Longitude in degrees of the transect's geometric centroid.	
	Ctr_Lat	**Geometric Centroid Latitude:** Latitude in degrees of the transect's geometric centroid.	
	LEnd_Lon	**Lower Endpoint Longitude:** Longitude in degrees of the transect's lower endpoint.	
	LEnd_Lat	**Lower Endpoint Latitude:** Latitude in degrees of the transect's lower endpoint.	
	LEnd_Elv	**Lower Endpoint Elevation:** Elevation in meters of the lower endpoint, derived from the AW3D30 global DSM dataset.	
	UEnd_Lon	**Upper Endpoint Longitude:** Longitude in degrees of the transect's upper endpoint.	
	UEnd_Lat	**Upper Endpoint Latitude:** Latitude in degrees of the transect's upper endpoint.	
	UEnd_Elv	**Upper Endpoint Elevation:** Elevation in meters of the upper endpoint, sourced from the AW3D30 global DSM dataset.	
	L_CanopyHt	**Lower Half Canopy Height:** Average canopy height in meters of the transect's lower half, based on Global Canopy Height 2020. May include "NA" for unavailable data.	
	L_NDVI	**Lower Half NDVI:** Average NDVI of the transect's lower half, derived from Landsat-8 OLI 2020 data. May contain "NA" due to image masking.	
	U_CanopyHt	**Upper Half Canopy Height:** Average canopy height in meters of the transect's upper half, from Global Canopy Height 2020. Includes "NA" for data unavailability.	
	U_NDVI	**Upper Half NDVI:** Average NDVI of the transect's upper half, based on Landsat-8 OLI 2020 data. "NA" values possible due to image masking.	
Watershed	HYBAS_ID	**Watershed Identifier:** Unique ID for the "Level 12" HydroSHEDS watershed at the transect's centroid, linking to the HydroSHEDS dataset.	
Mountain Range	GMBA_V2_ID	**GMBA Mountain Range Identifier:** Unique ID for the "Broad" GMBA mountain range at the transect's centroid, for linking with the "GMBA Inventory v2.0_broad" dataset.	

	GMBA_Name	**GMBA Mountain Range Name:** Derived from the "MapName" column in the "GMBA Inventory v2.0_broad" dataset.	"Alpine Treeline Elevational Transect Centroids_v1.0". **File Size:** 2.33 GB
	GMBA_Regn	**GMBA Continental Region Name:** Based on "Level_01" and "Level_02" columns of the "GMBA Inventory v2.0_broad" dataset.	
	GMBA_Ctr_X	**GMBA Centroid Longitude:** Longitude in degrees of the GMBA mountain range's geometric centroid.	
	GMBA_Ctr_Y	**GMBA Centroid Latitude:** Latitude in degrees of the GMBA mountain range's geometric centroid.	

Table 2. Attributes of Data in ATET_v1.0 (*Alpine Treeline Elevational Transects_v1.0*) and ATEC_v1.0 (*Alpine Treeline Elevational Transect Centroids_v1.0*).

Alpine Treeline Elevational Transect Centroids_v1.0 (ATEC_v1.0)
The ATEC_v1.0 vector dataset, detailed in Table 2, contains 2,312,022 points, each pinpointing the geometric centroid of an elevational transect from ATET_v1.0. This dataset mirrors the attributes of ATET_v1.0. It includes a unique identifier "ET_ID" for each centroid, allowing for the correlation of each centroid with its respective elevational transect in the ATET_v1.0 dataset.

Technical Validation

The ATET_v1.0/ATEC_v1.0 dataset was developed to map the transition from the treeless alpine tundra to lower-elevation montane forests within alpine treeline ecotones. To validate these global elevational transects, we assessed their effectiveness in capturing ecological changes, focusing on Vegetation Canopy Height (VCH) and primary productivity, using two data sources with 10-m and 30-m spatial resolutions. The R[48] code for the technical validation of these transects is available on Zenodo at https://zenodo.org/records/17428155.

Vegetation Canopy Height Analysis
We employed the 2020 global 10-m VCH dataset by Lang et al.[49], derived from Global Ecosystem Dynamics Investigation (GEDI) data and Sentinel-2 imagery, to measure vegetation heights within these ecotones (as displayed in Supplementary Fig. 1d). Each elevational transect was bisected at its geometric centroid to create equal-sized lower and upper segments (as shown by the red and blue polygons in Fig. 6d). The VCH for each 10-m pixel was averaged within these segments, resulting in "L_CanopyHt" and "U_CanopyHt" values for the lower and upper segments, respectively (as detailed in Table 2).

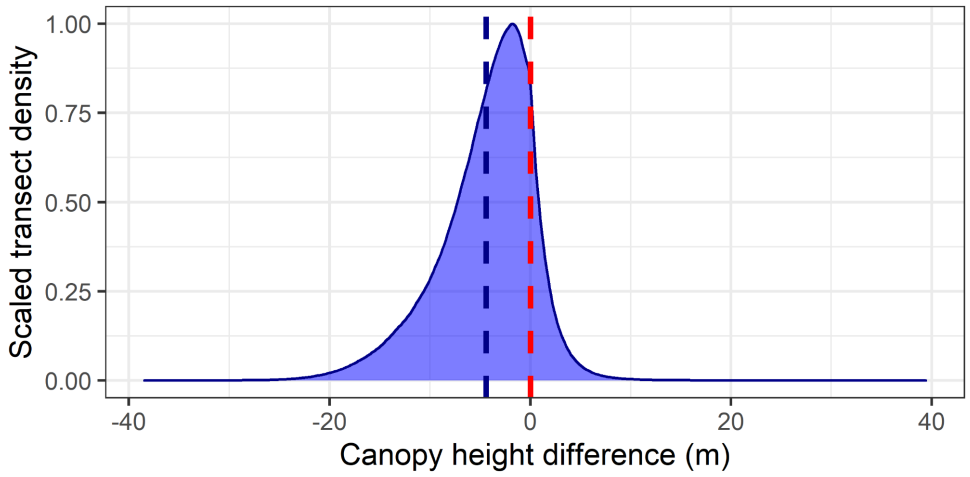

(a)

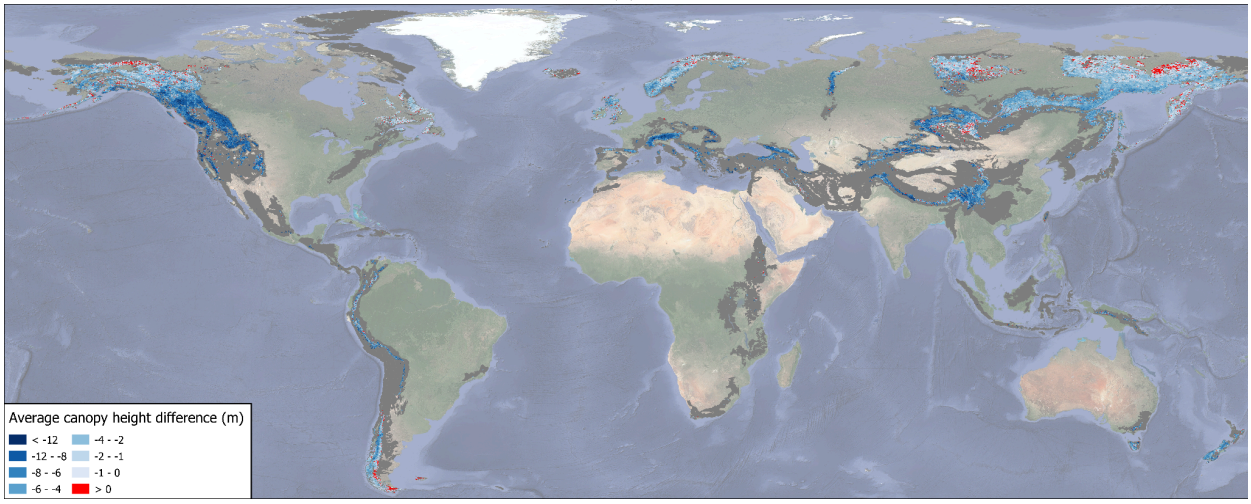

(b)

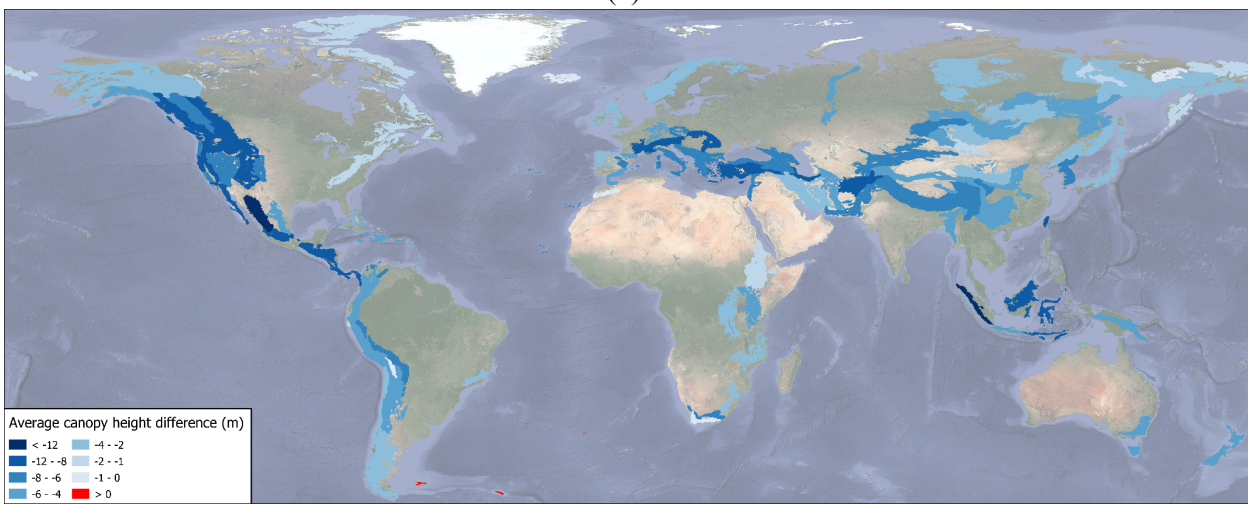

(c)

Fig. 4 Comparative Analysis of Vegetation Canopy Heights (VCHs) Across Elevational Transects. This figure presents the disparities in VCHs between the upper and lower segments of each elevational transect, analyzed at three distinct levels as defined in Eq. 1. Panel **(a)** illustrates the "Transect" level analysis, showcasing a scaled density plot along with the mean VCH difference, depicted by a dashed blue line, across transect segment pairs. Panel **(b)** focuses on the "Watershed" level, where the VCH difference values are averaged for all transects within each HydroSHEDS watershed. Panel **(c)** examines the "Mountain Range" level, displaying the mean VCH difference for all transects within each GMBA mountain range.

We computed the difference in canopy height between upper and lower segments (VCH_{diff}) using the formula:

$$VCH_{diff} = VCH_{upper} - VCH_{lower} \quad (1)$$

where VCH_{diff} is the height difference along a transect, with VCH_{upper} and VCH_{lower} representing the average heights of the upper and lower segments, respectively.

Our analysis showed that 85.52% of transects had higher VCH_{lower} than VCH_{upper} (refer to Fig. 4a), indicating a general decrease in canopy height by about 4.39 m when moving from lower to upper segments (as illustrated by the dashed blue line in Fig. 4a). Further, we averaged VCH_{diff} across all transects within each HydroSHEDS watershed and GMBA mountain range. As depicted in Fig. 4b,c, the average VCH_{diff} values were typically higher in tropical and temperate regions compared to high-latitude mountains. Consequently, this transect dataset effectively captures the variation in vegetation canopy structure along elevational gradients in alpine treeline ecotones globally. In addition, the observed positive average VCH_{diff} values at higher latitudes in the northern hemisphere, notably in regions like Alaska (as indicated by the red areas in Fig. 4b,c), may be attributed to significant uncertainties and tiling artifacts associated with the VCH data in these areas[49].

NDVI Analysis

The 30-m USGS Landsat imagery has proven instrumental in identifying and tracking the dynamics of alpine treeline ecotones in response to recent climate changes at both local and regional scales[10,37,38,50]. In this context, our study incorporated the Landsat-8 Operational Landsat Imager (OLI) Collection 1 Surface Reflectance (SR) data for 2020[51]. This data, processed using the Land Surface Reflectance Code[52,53], includes a detailed "cloud, cloud shadow, water, and snow" mask, as provided by the C Function of Mask[54]. We initially preprocessed the Landsat images by filtering out pixels that were either marked as high-confidence cloud cover, identified as cloud shadow, or missing in any band. Following this, we selected the SR bands ("Bands 1-7") and eliminated any pixels with reflectance values outside the 0-10,000 range.

The Normalized Difference Vegetation Index (NDVI)[55] is correlated with the fraction of photosynthetically active radiation absorbed by vegetation[56], making it a useful metric in remote-sensing analyses of vegetation growth and dynamics. Consequently, NDVI has been widely used as a proxy for assessing vegetation productivity and canopy mortality at broad scales[57–64]. In our study, we used the 2020 Landsat-derived NDVI to evaluate the efficacy of elevational transects in capturing the local variations in vegetation productivity within alpine treeline ecotones.

The NDVI for each pixel was computed from the preprocessed Landsat-8 SR images of 2020. To mitigate issues related to residual cloud cover, shadow, snow, or water[60], we extracted the annual maximum NDVI from each pixel for the land surface (as illustrated in Supplementary Fig. 1e). This approach also helped distinguish between vegetated and non-vegetated areas more clearly. Subsequently, we averaged the NDVI values of all 30-m pixels across each transect segment. The resulting data for each segment was labeled as "L_NDVI" and "U_NDVI" for the lower and upper segments, respectively (refer to Table 2).

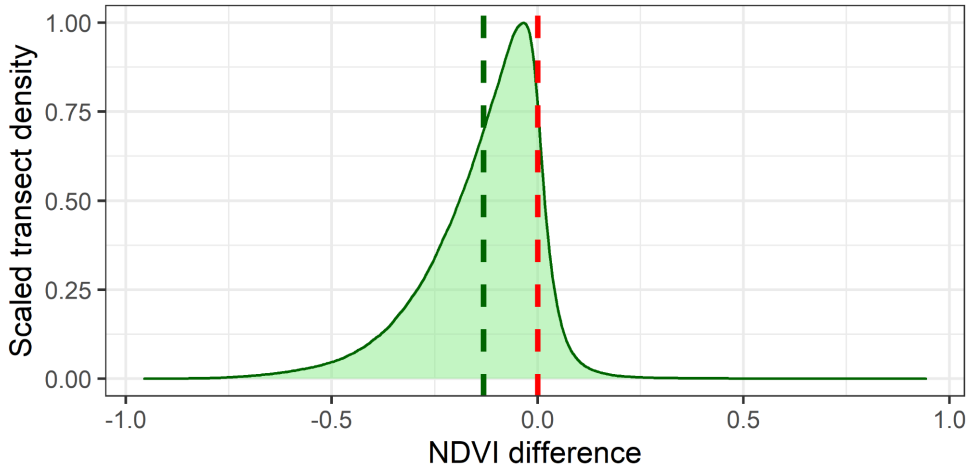

(a)

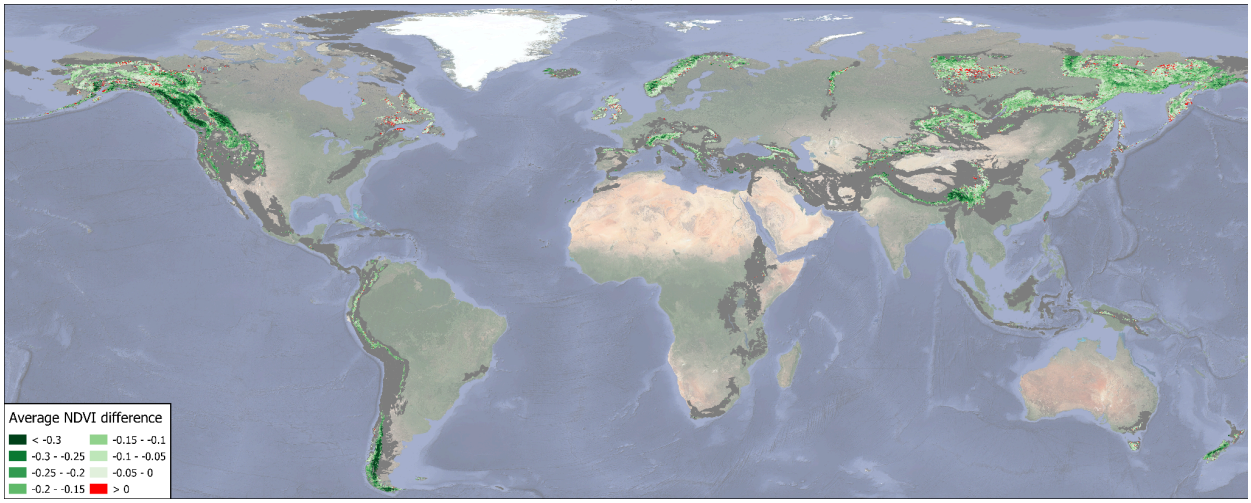

(b)

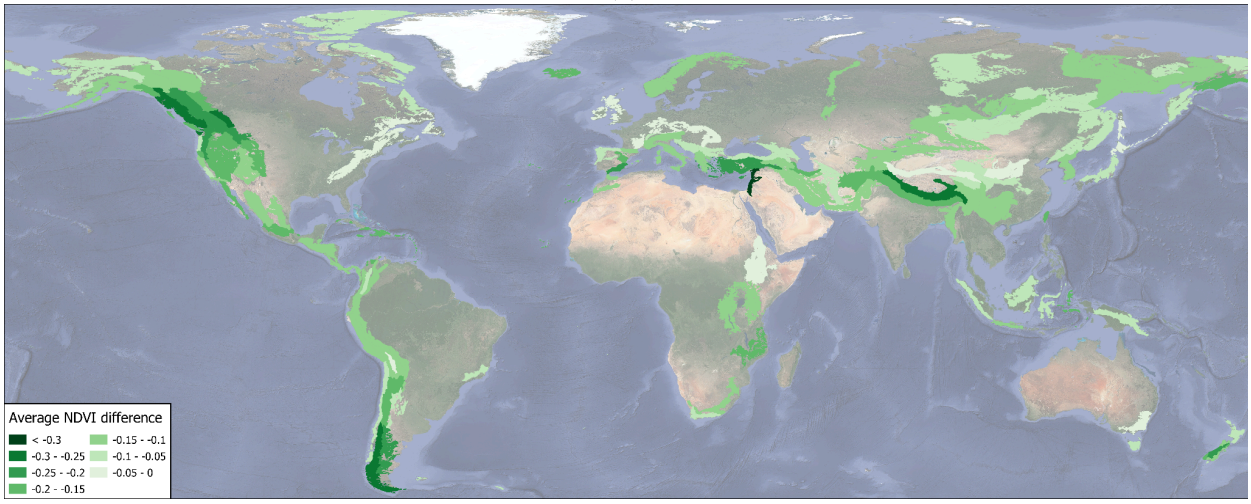

(c)

Fig. 5 Comparative Analysis of NDVI Differences Across Elevational Transects. This figure illustrates the variations in Normalized Difference Vegetation Indices (NDVIs) between the upper and lower segments of each elevational transect at three distinct levels (refer to Eq. 2). Panel **(a)** at the

"Transect" level: scaled density plot along with the mean NDVI difference (indicated by a dashed green line) for each transect segment pair. Panel **(b)** at the "Watershed" level: average NDVI difference computed across all elevational transects within each HydroSHEDS watershed. Panel **(c)** at the "Mountain Range" level: mean NDVI difference for all elevational transects within each GMBA mountain range.

To further understand vegetation changes along the transects, we calculated the NDVI difference between each transect's upper and lower segments as follows:

$$NDVI_{diff} = NDVI_{upper} - NDVI_{lower} \quad (2)$$

Here, $NDVI_{diff}$ represents the NDVI difference along an elevational transect, with $NDVI_{upper}$ and $NDVI_{lower}$ denoting the average NDVI values of the upper and lower segments, respectively.

Our analysis revealed that in about 88.39% of the transects, the $NDVI_{lower}$ exceeded $NDVI_{upper}$ (as referenced in Fig. 5a). Typically, NDVI decreased by approximately 0.13 from the lower to the upper segment along an elevational gradient (refer to the dashed green line in Fig. 5a). Additionally, we averaged the $NDVI_{diff}$ values across all transects within each HydroSHEDS watershed and GMBA mountain range. As shown in Fig. 5b,c, the average $NDVI_{diff}$ values were generally higher in mid-latitude mountains compared to other regions, indicating that our transect dataset effectively captured the local shifts in vegetation productivity from montane closed forests to adjacent non-forested areas.

Transect Length and Orientation Assessment

To validate the precision of our elevational transects for depicting local ecological shifts in global alpine treeline ecotones, we conducted an assessment of transect length and orientation. Initially, for comprehensive geographic representation in our validation process, we selected one transect randomly from each of the 66,776 HydroSHEDS watersheds, which encompass the ATEs worldwide. Subsequently, we altered the sizes and directions of these chosen transects. This step was essential to evaluate how such changes impact the precise mapping of variations in two key indicators: vegetation canopy height and greenness index. The vector datasets for transect assessment can be accessed on Zenodo at https://zenodo.org/records/10739392. Our expectation was that changing the length or orientation of an elevational transect would result in smaller variations in both variables across the transect. This would indicate that the determined transect lengths and directions optimally capture the vegetational changes within alpine treeline ecotones along local elevational gradients.

Assessing the Influence of Transect Size Adjustments

To modify the length of each sampled elevational transect, we altered the endpoint coordinates using the formula outlined in Eq. 3.

$$\begin{bmatrix} x' - x_c \\ y' - y_c \end{bmatrix} = r \cdot \begin{bmatrix} x - x_c \\ y - y_c \end{bmatrix} \quad (3)$$

This equation utilizes the original longitude (x) and latitude (y) of the transect's endpoints (either "LEnd_Lon/Lat" or "UEnd_Lon/Lat" from Table 2), and the transect's geometric centroid coordinates (x_c and y_c, as noted in the "Ctr_Lon/Lat" fields of Table 2). The variables x' and y' represent the adjusted longitude and latitude, respectively. The ratio (r) signifies the proportion between the modified and original transect lengths. We examined seven distinct r values: 0.125, 0.25, 0.5, 1, 2, 4, and 8, as demonstrated in Fig. 6a,b. The original transects are indicated by "r = 1" (gray polygons in Fig. 6a,b),

while the extended transects correspond to r values of 2, 4, and 8 (non-gray polygons in Fig. 6a), and the shortened ones to "r = 0.125/0.25/0.5" (non-gray polygons in Fig. 6b).

To analyze local vegetation productivity variations along the elevational gradient, each altered transect was bisected at its geometric center, as shown in Fig. 6d. Transects shorter than 90 m (the transect width) were excluded to ensure the resulting segments were greater than zero meters. The elevation data within these adjusted transects varied significantly, particularly in those with high r values, due to the complex mountain topography. We identified the upper and lower transect segments by comparing their ALOS elevation averages. For all modified transects, we calculated the differences in average VCH and NDVI between each segment pair using Eq. 1 and Eq. 2, generating 45,872 transect samples across all seven size adjustment ratios.

As indicated in Fig. 6e, the median values of both VCH and NDVI differences are negative for all transect adjustment groups, suggesting a general decline in vegetation canopy height and greenness index with increasing elevation in mountainous areas. Among the seven length adjustment categories, the absolute medians of VCH and NDVI differences peak at 4.51 m and 0.125, respectively, when transects are extended to twice their original length (r = 2). This increase, compared to the original transects (3.73 m for "VCH difference" and 0.101 for "NDVI difference"), may result from the expanded coverage of non-vegetated and forested areas at higher and lower elevations, respectively, in the extended transects (blue polygon in Fig. 6a). However, those longer transects with r values of 4 and 8, may cross multiple hillslopes (green and red polygons in Fig. 6a), potentially leading to a reduction in VCH and NDVI differences between the upper and lower segments (Fig. 6e). Additionally, these extended transects may be more susceptible to anthropogenic influences, affecting the accuracy of representing ecological transitions in mountainous environments.

Conversely, as transect sizes decrease (r < 1, as shown in non-gray polygons in Fig. 6b), the similarity in vegetation coverage between their higher and lower parts increases, leading to reduced variability in canopy height and greenness index. As a result, the absolute medians of both VCH and NDVI differences diminish to their lowest values (0.45 m for "VCH difference" and 0.011 for "NDVI difference") when the length adjustment ratio is at its minimum (r = 0.125), as illustrated in Fig. 6e.

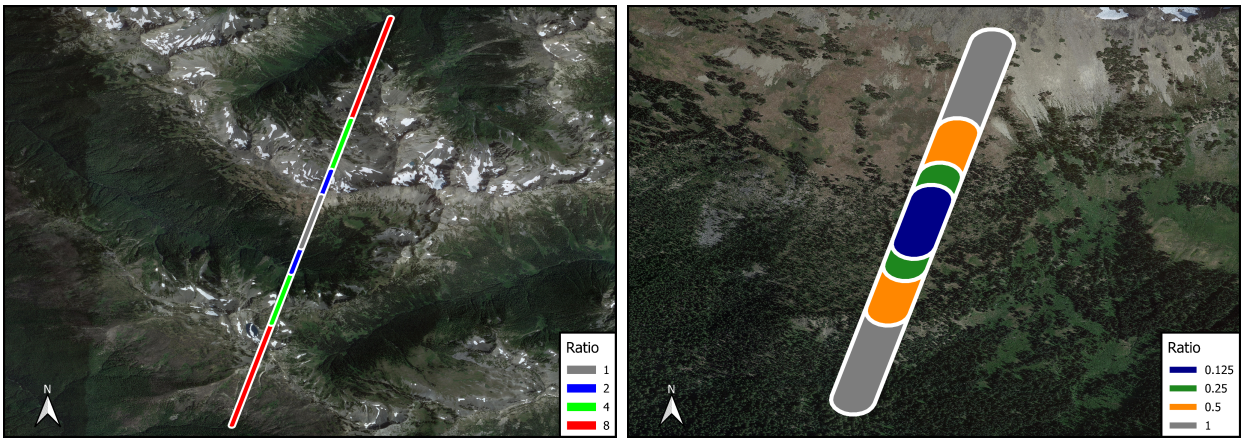

(a) (b)

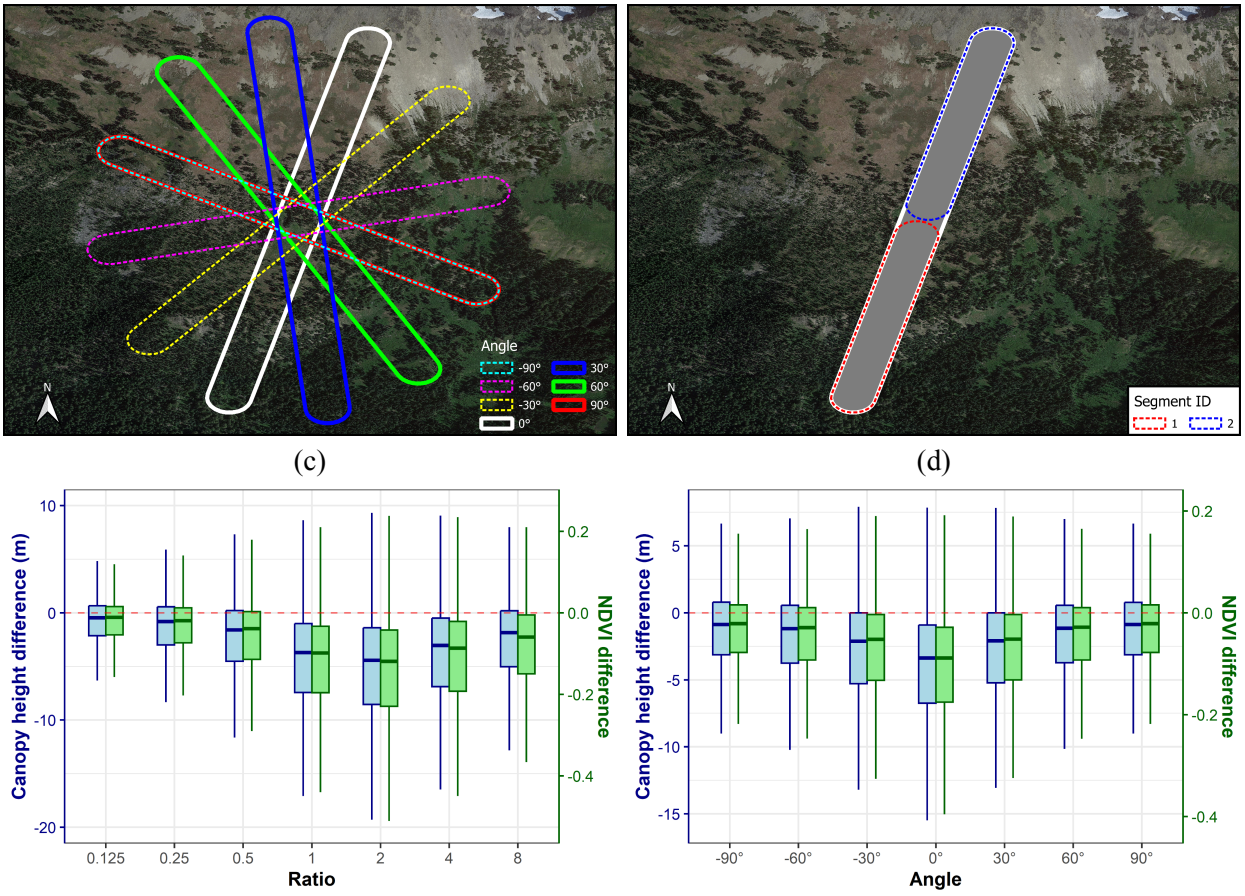

Fig. 6 Modifications and Impacts on Sampled Elevational Transects. This figure demonstrates the adjustments made to elevational transects globally selected from each "Level 12" HydroSHEDS watershed encompassing alpine treeline ecotones. Panels **(a)** to **(d)** illustrate the changes to a transect in Olympic National Park, Washington, USA. Panels **(a)** and **(b)** display variations in transect length, with the ratio (r) ranging from 0.125 to 8, showcasing comparative overlays of variously extended or shortened transects. Panel **(c)** shows angle (θ) adjustments between -90° to 90°, with negative and positive values indicating clockwise and counter-clockwise rotations, respectively. Panel **(d)** highlights transect segmentation into lower and upper parts, labeled "1" (with a red border) and "2" (with a blue border). Panels **(e)** and **(f)** feature box plots that analyze the disparities in Vegetation Canopy Height (VCH) and Normalized Difference Vegetation Index (NDVI) between the segmented parts of each modified transect globally, categorized by size ratio (r) or rotation angle (θ). These plots contain blue and green boxes (for "VCH difference" and "NDVI difference", respectively) with whiskers, and a red dashed line indicating no difference. Values outside 1.5 times the interquartile range from the quartiles are marked as outliers and not included in these plots.

Assessing the Influence of Transect Direction Adjustments

To modify the orientation of each sampled elevational transect, we used a specific formula to recalibrate the endpoint coordinates:

$$\begin{bmatrix} x' - x_c \\ y' - y_c \end{bmatrix} = \begin{bmatrix} \cos\theta & -\sin\theta \\ \sin\theta & \cos\theta \end{bmatrix} \begin{bmatrix} x - x_c \\ y - y_c \end{bmatrix} \tag{4}$$

This equation employs variables x, y, x', y', x_c, and y_c, consistent with those in Eq. 3. In Eq. 4, θ signifies the angular difference between the modified and initial transect directions. This angle varies across seven distinct values: -90°, -60°, -30°, 0°, 30°, 60°, and 90°, as illustrated in Fig. 6c. The "θ = 0°" condition reflects the unaltered transect (as shown by the white polygon in Fig. 6c), while positive angles (θ = 30°/60°/90°, illustrated by non-white solid-line polygons in Fig. 6c) indicate a counter-clockwise shift. Conversely, negative values (θ = -90°/-60°/-30°, depicted by non-white dotted-line polygons in Fig. 6c) represent a clockwise shift. Notably, transects rotated to "θ = 90°" and "θ = -90°" are equivalent, as seen with the red and cyan polygons in Fig. 6c.

To assess local vegetation coverage changes along the elevational gradient, we divided each rotated transect at its geometric midpoint (example in Fig. 6d). Given the complex topography of mountain regions, we compared average ALOS elevation data for each transect segment pair to ascertain their relative elevations. We then calculated the difference in average VCH and NDVI between the upper and lower segments of each transect (refer to Eq. 1 and Eq. 2).

In our analysis of 66,345 transect samples, encompassing all seven orientation adjustments, we observed negative median differences in both vegetation canopy height and greenness index for each rotation category, indicating a decrease in these variables with elevation (refer to Fig. 6f). The absolute median values of these differences peaked (3.49 m for "VCH difference" and 0.093 for "NDVI difference") with no transect rotation (θ = 0°). As Fig. 6c demonstrates, increased rotation angles result in more similar vegetation coverage between the higher and lower zones of the transects, particularly when rotations reach ±90° (red and cyan polygons in Fig. 6c). Consequently, as θ grows from 0° to ±90°, the absolute medians of both VCH and NDVI differences decrease, reaching their lowest at 0.82 m and 0.021, respectively, for rotations of -90° or 90° (as shown in Fig. 6f).

Our global transect sample assessment confirmed that original, unadjusted transects most accurately represent the elevational variation in canopy structure and vegetation productivity, spanning from montane closed forests to adjacent treeless alpine regions worldwide, at a local scale.

Usage Notes

Additional Information and Spatial Aggregation

The ATET_v1.0 (Alpine Treeline Elevational Transects_v1.0) dataset not only includes basic properties of the elevational transects but also offers additional attributes for enhanced spatial analysis. These attributes, listed as "HYBAS_ID" and "GMBA_V2_ID" in Table 2, link each transect with corresponding records in the HydroSHEDS "Level 12" data[45,46] and the "GMBA Inventory v2.0_broad" dataset[42,43]. This linkage allows users to access hydrological and geographic details relevant to the transects. As Fig. 4b,c and Fig. 5b,c illustrate, these attributes enable the aggregation of collected variables (like vegetation canopy height and greenness index) from a local scale (elevational transect) to broader scales (watershed, mountain range, or continental region). This aggregation facilitates comparisons or integration with similar data products. For more complex spatial operations, such as merging transects with other datasets, the ATEC_v1.0 (Alpine Treeline Elevational Transect Centroids_v1.0) can be used to represent transect locations and assess spatial relationships with other data.

Spatial Coverage

Before using the ATET_v1.0 dataset, users should verify if their study area overlaps with the elevational transects and their geometric centroids defined in the dataset, using the Google Earth Engine web application accessible at https://zenodo.org/records/10739392 (refer to Supplementary File 1). Additionally, some incorporated datasets, like the ALOS Landform data product, have lower quality in high-latitude regions. Users are advised to scrutinize spatial coverage for transects in these areas more closely.

Known Limitations
The elevational transects in the ATET_v1.0 dataset exhibit uneven spatial distribution due to the complex topography of mountain regions, leading to clustering or scattering in certain areas. Users requiring uniform distribution can perform spatial "thinning" operations, like random selection or averaging observations over a defined area (e.g., 1 km^2).

Elongating transects beyond their defined endpoints is not feasible in the current dataset. However, future updates may introduce additional transect types like nival, alpine, montane, and "valley-to-peak" transects to address this limitation.

Finally, due to the varying lengths and orientations of the transects, establishing topological relations with other spatial datasets can be challenging. A solution is to use coordinates of a relevant point feature (geometric centroid, lower or upper endpoint) from the ATET_v1.0/ATEC_v1.0 datasets to represent each transect's spatial location.

Code Availability
The JavaScript code for constructing the Alpine Treeline Elevational Transects_v1.0 (ATET_v1.0) within Olympic National Park, Washington, USA, using Google Earth Engine is accessible at https://zenodo.org/records/17428155. This code can be easily adapted to replicate the process for alpine treeline ecotones in other study areas. Additionally, the JavaScript code for visualizing the complete ATET_v1.0 and Alpine Treeline Elevational Transect Centroids_v1.0 (ATEC_v1.0) datasets, along with relevant details, is available at the same Zenodo URL. This code enables user interaction with the datasets through Google Earth Engine. The R code for technical validation of the elevational transects is also hosted on Zenodo at the same link.

Funding
This work was supported by NASA Headquarters under the NASA Earth and Space Science Fellowship Program - Grant 80NSSC18K1401.

Author Contributions
Chenyang Wei: conceptualization; methodology; investigation; writing (original draft); writing (review and editing); visualization; and funding acquisition.

Adam M. Wilson: conceptualization; resources; writing (review and editing); supervision; project administration; and funding acquisition.

Competing Interests
The authors declare no competing interests.

References
1. Körner, C. *Alpine Treelines: Functional Ecology of the Global High Elevation Tree Limits*. (Springer Basel, 2012).
2. Paulsen, J. & Körner, C. A climate-based model to predict potential treeline position around the globe. *Alpine Botany* **124**, 1–12 (2014).
3. Graham, C. H. *et al.* The origin and maintenance of montane diversity: integrating evolutionary and ecological processes. *Ecography* **37**, 711–719 (2014).
4. Sundqvist, M. K., Sanders, N. J. & Wardle, D. A. Community and Ecosystem Responses to Elevational Gradients: Processes, Mechanisms, and Insights for Global Change. *Annu. Rev. Ecol. Evol. Syst.* **44**, 261–280 (2013).

5. Körner, C. *Alpine Treelines: Functional Ecology of the Global High Elevation Tree Limits*. (Springer Science & Business Media, 2012).
6. Körner, C., Paulsen, J. & Spehn, E. M. A definition of mountains and their bioclimatic belts for global comparisons of biodiversity data. *Alp Botany* **121**, 73 (2011).
7. Goody, R. M., Walker, J. C. G., Goodwin, R. M. & Walker, J. C. *Atmospheres (Foundations of Earth Science Series)*. (Prentice-Hall, 1972).
8. Minder, J. R., Mote, P. W. & Lundquist, J. D. Surface temperature lapse rates over complex terrain: Lessons from the Cascade Mountains. *J. Geophys. Res.* **115**, F02011 (2010).
9. Wei, C. Global Alpine Treeline Ecotone Dynamics Under Climate Change. (State University of New York at Buffalo, Ann Arbor, United States, 2023).
10. Wei, C., Karger, D. N. & Wilson, A. M. Spatial detection of alpine treeline ecotones in the Western United States. *Remote Sens. Environ.* **240**, 111672 (2020).
11. Körner, C. A re-assessment of high elevation treeline positions and their explanation. *Oecologia* **115**, 445–459 (1998).
12. Körner, C. The cold range limit of trees. *Trends Ecol. Evol.* **36**, 979–989 (2021).
13. Körner, C. & Hoch, G. Not every high‐latitude or high‐elevation forest edge is a treeline. *J. Biogeogr.* (2023) doi:10.1111/jbi.14593.
14. Mayor, J. R. *et al.* Elevation alters ecosystem properties across temperate treelines globally. *Nature* **542**, 91–95 (2017).
15. Kullman, L. & Oberg, L. Post-Little Ice Age tree line rise and climate warming in the Swedish Scandes: a landscape ecological perspective. *J. Ecol.* **97**, 415–429 (2009).
16. Hertel, D. & Scholing, D. Norway Spruce Shows Contrasting Changes in Below- Versus Above-Ground Carbon Partitioning towards the Alpine Tree line: Evidence from a Central European Case Study. *Arct. Antarct. Alp. Res.* **43**, 46–55 (2011).
17. Qi, Z., Liu, H., Wu, X. & Hao, Q. Climate-driven speedup of alpine treeline forest growth in the Tianshan Mountains, Northwestern China. *Glob. Chang. Biol.* **21**, 816–826 (2015).
18. Shrestha, K. B., Hofgaard, A. & Vandvik, V. Recent treeline dynamics are similar between dry and mesic areas of Nepal, central Himalaya. *JOURNAL OF PLANT ECOLOGY* **8**, 347–358 (2015).
19. Bello-Rodriguez, V., Cubas, J., Del Arco, M. J., Martin, J. L. & Gonzalez-Mancebo, J. M. Elevational and structural shifts in the treeline of an oceanic island (Tenerife, Canary Islands) in the context of global warming. *Int. J. Appl. Earth Obs. Geoinf.* **82**, (2019).
20. Hagedorn, F. *et al.* Latitudinal decline in stand biomass and productivity at the elevational treeline in the Ural mountains despite a common thermal growth limit. *J. Biogeogr.* **47**, 1827–1842 (2020).
21. Oberhuber, W. *et al.* Growth Trends of Coniferous Species along Elevational Transects in the Central European Alps Indicate Decreasing Sensitivity to Climate Warming. *For. Trees Livelihoods* **11**, (2020).
22. Zhou, W. *et al.* Spatiotemporal dynamics of encroaching tall vegetation in timberline ecotone of the Polar Urals Region, Russia. *Environ. Res. Lett.* **17**, 014017 (2021).
23. Lu, X. *et al.* Loss of growth resilience towards the alpine shrubline. *For. Ecol. Manage.* **539**, 121013 (2023).
24. Gorelick, N. *et al.* Google Earth Engine: Planetary-scale geospatial analysis for everyone. *Remote Sens. Environ.* **202**, 18–27 (2017).
25. Malanson, G. P. *et al.* Alpine Treeline of Western North America: Linking Organism-To-Landscape Dynamics. *Phys. Geogr.* **28**, 378–396 (2007).
26. Karagulle, D. *et al.* Modeling global Hammond landform regions from 250-m elevation data. *Trans. GIS* **21**, 1040–1060 (2017).
27. Sayre, R. *et al.* A New High-Resolution Map of World Mountains and an Online Tool for Visualizing and Comparing Characterizations of Global Mountain Distributions. *mred* **38**, 240–249 (2018).
28. Karger, D. N. *et al.* Climatologies at high resolution for the earth's land surface areas. *Sci Data* **4**, 170122 (2017).
29. Karger, D. N. *et al.* Why tree lines are lower on islands—Climatic and biogeographic effects hold the

answer. *Glob. Ecol. Biogeogr.* **28**, 839–850 (2019).
30. Danielson, J. J. & Gesch, D. B. *Global Multi-Resolution Terrain Elevation Data 2010 (GMTED2010)*. https://pubs.er.usgs.gov/publication/ofr20111073 (2011).
31. Pepin, N. *et al.* Elevation-dependent warming in mountain regions of the world. *Nat. Clim. Chang.* **5**, 424–430 (2015).
32. Pepin, N. C. *et al.* Climate changes and their elevational patterns in the mountains of the world. *Rev. Geophys.* **60**, (2022).
33. Takaku, J., Tadono, T., Tsutsui, K. & Ichikawa, M. VALIDATION OF'AW3D'GLOBAL DSM GENERATED FROM ALOS PRISM. *ISPRS Annals of Photogrammetry, Remote Sensing & Spatial Information Sciences* **3**, (2016).
34. Takaku, J., Tadono, T., Doutsu, M., Ohgushi, F. & Kai, H. Updates of 'aw3d30' Alos global digital surface model with other open access datasets. *ISPRS - Int. Arch. Photogramm. Remote Sens. Spat. Inf. Sci.* **XLIII-B4-2020**, 183–189 (2020).
35. Tadono, T. *et al.* Generation of the 30 M-Mesh Global Digital Surface Model by Alos Prism. *ISPRS - International Archives of the Photogrammetry, Remote Sensing and Spatial Information Sciences* **41B4**, 157 (2016).
36. Uuemaa, E., Ahi, S., Montibeller, B., Muru, M. & Kmoch, A. Vertical Accuracy of Freely Available Global Digital Elevation Models (ASTER, AW3D30, MERIT, TanDEM-X, SRTM, and NASADEM). *Remote Sensing* **12**, 3482 (2020).
37. Tian, L., Fu, W., Tao, Y., Li, M. & Wang, L. Dynamics of the alpine timberline and its response to climate change in the Hengduan mountains over the period 1985–2015. *Ecol. Indic.* **135**, 108589 (2022).
38. Zou, F. *et al.* Alpine Treeline Dynamics and the Special Exposure Effect in the Hengduan Mountains. *Frontiers in Plant Science* vol. 13 Preprint at https://doi.org/10.3389/fpls.2022.861231 (2022).
39. Buchhorn, M. *et al.* Copernicus Global Land Cover Layers—Collection 2. *Remote Sensing* **12**, 1044 (2020).
40. Di Gregorio, A. & Food and Agriculture Organization of the United Nations. *Land Cover Classification System: Classification Concepts and User Manual : LCCS*. (Food & Agriculture Org., 2005).
41. Blyth, S., Lysenko, I., Groombridge, B., Miles, L. & Newton, A. Mountain watch: environmental change and sustainable development in mountains. (2002).
42. Snethlage, M. A. *et al.* A hierarchical inventory of the world's mountains for global comparative mountain science. *Sci Data* **9**, 149 (2022).
43. Snethlage, M. A. *et al.* GMBA mountain inventory v2. GMBA-EarthEnv (2021).
44. Hansen, M. C. *et al.* High-resolution global maps of 21st-century forest cover change. *Science* **342**, 850–853 (2013).
45. Lehner, B., Verdin, K. & Jarvis, A. New global hydrography derived from spaceborne elevation data. *Eos* **89**, 93 (2008).
46. Lehner, B. & Grill, G. Global river hydrography and network routing: baseline data and new approaches to study the world's large river systems. *Hydrol. Process.* **27**, 2171–2186 (2013).
47. Theobald, D. M., Harrison-Atlas, D., Monahan, W. B. & Albano, C. M. Ecologically-Relevant Maps of Landforms and Physiographic Diversity for Climate Adaptation Planning. *PLoS One* **10**, e0143619 (2015).
48. R Core Team. R: A Language and Environment for Statistical Computing. Preprint at https://www.R-project.org/ (2024).
49. Lang, N., Jetz, W., Schindler, K. & Wegner, J. D. A high-resolution canopy height model of the Earth. *Nat Ecol Evol* **7**, 1778–1789 (2023).
50. Xu, D., Geng, Q., Jin, C., Xu, Z. & Xu, X. Tree Line Identification and Dynamics under Climate Change in Wuyishan National Park Based on Landsat Images. *Remote Sensing* **12**, 2890 (2020).
51. Earth Resources Observation and Science (EROS) Center. Collection-1 U.S. Landsat Analysis Ready

Data (ARD) Level-2 Data Product. U.S. Geological Survey https://doi.org/10.5066/F7319TSJ (2017).
52. Vermote, E., Justice, C., Claverie, M. & Franch, B. Preliminary analysis of the performance of the Landsat 8/OLI land surface reflectance product. *Remote Sens. Environ.* **185**, 46–56 (2016).
53. U.S. Geological Survey. Landsat 8 Collection 1 (C1) Land Surface Reflectance Code (LaSRC) Product Guide. Preprint at (2020).
54. Foga, S. *et al.* Cloud detection algorithm comparison and validation for operational Landsat data products. *Remote Sens. Environ.* **194**, 379–390 (2017).
55. Rouse, J. W., Jr, Haas, R. H., Schell, J. A. & Deering, D. W. Monitoring Vegetation Systems in the Great Plains with Erts. in *NASA Special Publication* vol. 351 309 (1974).
56. Asrar, G., Fuchs, M., Kanemasu, E. T. & Hatfield, J. L. Estimating Absorbed Photosynthetic Radiation and Leaf Area Index from Spectral Reflectance in Wheat1. *Agron. J.* **76**, 300–306 (1984).
57. Myneni, R. B., Keeling, C. D., Tucker, C. J., Asrar, G. & Nemani, R. R. Increased plant growth in the northern high latitudes from 1981 to 1991. *Nature* **386**, 698 (1997).
58. Goetz, S. J., Bunn, A. G., Fiske, G. J. & Houghton, R. A. Satellite-observed photosynthetic trends across boreal North America associated with climate and fire disturbance. *Proc. Natl. Acad. Sci. U. S. A.* **102**, 13521–13525 (2005).
59. Olthof, I. & Pouliot, D. Treeline vegetation composition and change in Canada's western Subarctic from AVHRR and canopy reflectance modeling. *Remote Sens. Environ.* **114**, 805–815 (2010).
60. Pettorelli, N. *et al.* Using the satellite-derived NDVI to assess ecological responses to environmental change. *Trends Ecol. Evol.* **20**, 503–510 (2005).
61. Wang, X. *et al.* Spring temperature change and its implication in the change of vegetation growth in North America from 1982 to 2006. *Proc. Natl. Acad. Sci. U. S. A.* **108**, 1240–1245 (2011).
62. Berner, L. T. *et al.* Summer warming explains widespread but not uniform greening in the Arctic tundra biome. *Nat. Commun.* **11**, 1–12 (2020).
63. Berner, L. T. & Goetz, S. J. Satellite observations document trends consistent with a boreal forest biome shift. *Glob. Chang. Biol.* (2022) doi:10.1111/gcb.16121.
64. Testolin, R., Attorre, F. & Jiménez‐Alfaro, B. Global distribution and bioclimatic characterization of alpine biomes. *Ecography* **358**, 635 (2020).

Supplementary Information

Gridded Datasets in Alpine Treeline Ecotone Research

Gridded datasets, a prevalent type of remotely sensed data, are widely utilized in ecological and environmental research at regional and global scales. These datasets offer a uniform spatial arrangement at a specified resolution, enhancing the efficiency of spatial operations like aggregation and partitioning. This uniformity also facilitates straightforward comparisons and integrations of analyses across different datasets focusing on similar themes or locations. However, the fixed arrangement of gridded data presents challenges in analyzing spatially complex units, particularly those involving alpine treeline ecotones. This rigidity may have a negative impact on the accuracy and reliability of ATE analyses, as highlighted in Table 1. Firstly, in alpine treeline ecotones, the local aspect can vary significantly, making it challenging to capture precise environmental conditions with gridded datasets. For instance, a single pixel in such a dataset might encompass multiple hillslopes (as illustrated in Pixels 6 and 7 in Supplementary Fig. 1), possibly leading to the oversight of crucial sub-pixel variations like microclimate, topography, and vegetation coverage. Furthermore, these sub-pixel features' spatial patterns might be obscured, as only one value per pixel is typically recorded.

Secondly, the intricate topography of alpine treeline ecotones complicates the spatial representativeness of fixed-size pixels for assessing environmental conditions and ecological processes. While a pixel might be adequately sized for covering an ATE on one hillslope (e.g., Pixel 1 in Supplementary Fig. 1), it could be either too fine to capture the ecological transition from montane forest to alpine tundra (as seen in Pixels 2 and 3 in Supplementary Fig. 1d,e), or too coarse for isolating environmental data from a single hillside (e.g., Pixels 4 and 5 in Supplementary Fig. 1d,e).

Finally, due to the common conical shape of mountains, the area of an alpine treeline ecotone typically diminishes with increasing elevation. As a result, gridded data, with its fixed geometry, tends to cover more lowland than highland areas in ATEs (such as Pixel 8 in Supplementary Fig. 1c). This disproportion may lead to a dominance of low-elevation zones in data analysis, potentially skewing results towards these areas.

Interactive Web Application

We created an interactive web application hosted on Google Earth Engine, accessible at https://zenodo.org/records/10739392. This tool enables users to explore the spatial extent of the elevational transect dataset in their study areas and find applications customized for their research requirements.

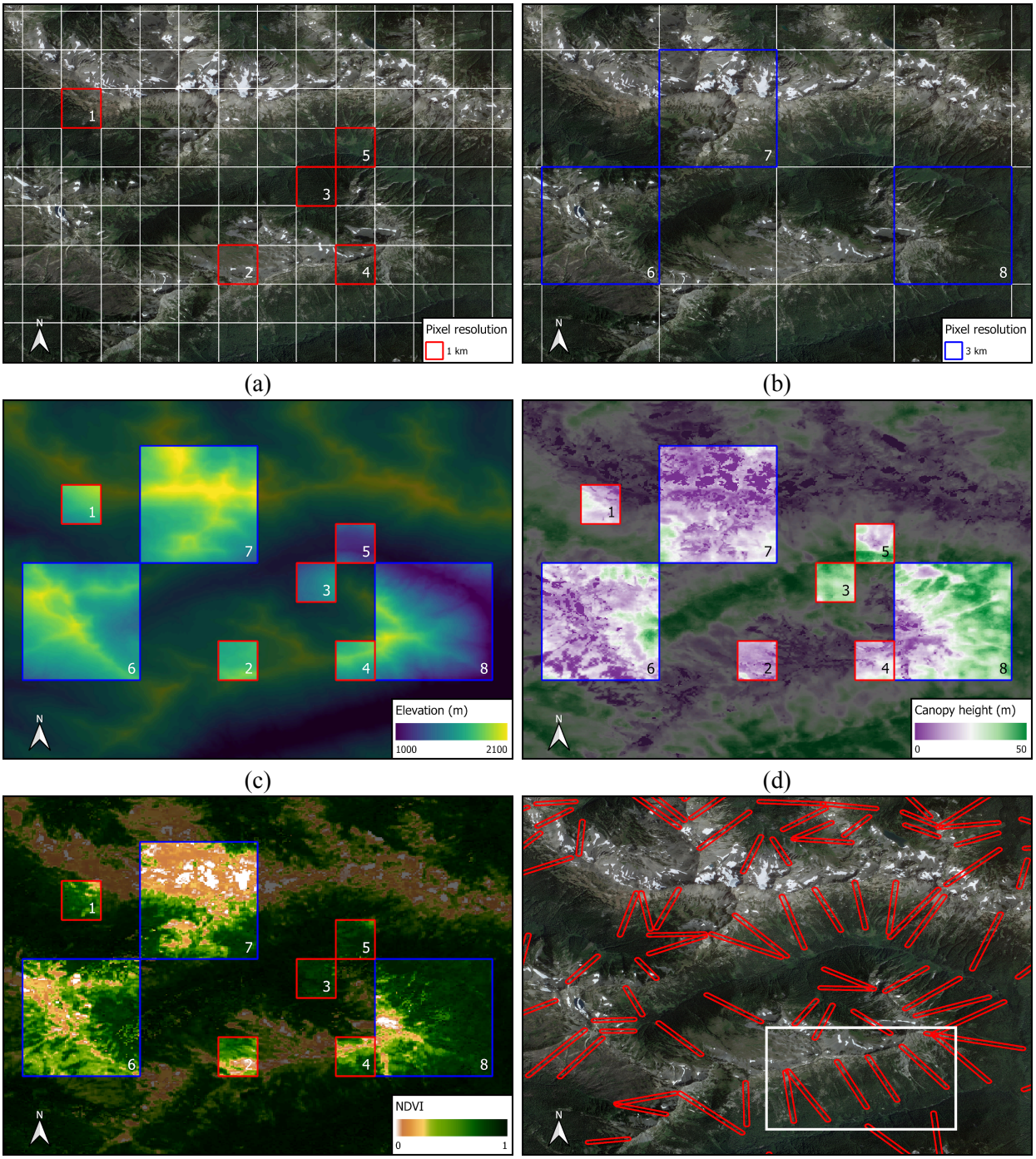

Supplementary Fig. 1 Comparative Visualization of Gridded Datasets and Environmental Variables in Olympic National Park, Washington, USA. This figure showcases two different resolutions of gridded datasets and their associated environmental variables. Panel **(a)** presents a 1-km resolution gridded dataset overlaying high-resolution Google satellite imagery, highlighting five specific pixels (Pixels 1-5). Panel **(b)** depicts a 3-km resolution gridded dataset with three distinct pixels (Pixels 6-8) identified. Panels **(c)** to **(e)** illustrate three key environmental variables within the boundaries of the selected pixels, using color coding for clarity (red for 1 km, blue for 3 km). These variables include: AW3D30 DSM elevation at

30-m precision (c), 2020 canopy height at 10-m based on Global Ecosystem Dynamics Investigation (GEDI) data and Sentinel-2 imagery (d), and the maximum Landsat-derived NDVI at 30-m for 2020 (e). Panel **(f)** outlines the elevational transects (shown as red polygons) and a designated hillside (white rectangle), with a detailed three-dimensional representation of the transect construction process provided in Fig. 4. Refer to Table 1 for detailed interpretations of the various regions depicted.